RSC Advances

PAPER

Cite this: *RSC Adv.*, 2014, **4**, 34369

# Combined influences of viscous fingering and solvent effect on the distribution of adsorbed solutes in porous media

Chinar Rana,[a] Anne De Wit,[b] Michel Martin[c] and Manoranjan Mishra*[a]

The displacement of two fluids in a porous medium can be affected by a viscous fingering instability (VF) that arises at the interface between the fluids when their viscosities are different. In parallel, one of the fluids may contain solutes that reversibly adsorb on the porous matrix at a rate that depends on the composition of the two-fluid mixture, a so-called solvent strength effect. In some systems encountered for instance in liquid chromatographic columns or in underground flows in environmental applications, both VF and solvent strength effects may combine to influence the spatio-temporal distribution of solutes. Here, a computational investigation of such dynamics is performed. The distribution of the solute in the porous medium is affected by the combined effects of VF and solvent strength. A three component system (displacing fluid, sample solvent and solute) is modeled using Darcy's law for the fluid flow velocity coupled to a convection–diffusion equation for the sample solvent and a mass balance equation for the solute in the mobile and stationary phases. The sample solvent is assumed to have a larger solvent strength than the displacing fluid, in which the retention parameter due to the linear adsorption of the solute depends exponentially on the concentration of the sample solvent. A parametric study of the influences of the factors controlling the VF and solvent strength effects on the displacement velocity of the fronts of solute zone and on its width along the porous medium has been performed by direct numerical simulation of the governing equations. While each of the two effects (VF and solvent strength effects) distorts and significantly increases the broadening of the solute zone, the simulations reveal that, when they are acting in combination, these solute zone perturbations are reduced.

Received 6th March 2014
Accepted 21st July 2014

DOI: 10.1039/c4ra01965b

www.rsc.org/advances

## 1 Introduction

Viscous fingering (VF) is a hydrodynamic instability observed when a less viscous fluid displaces a more viscous one in a porous medium or in a Hele-Shaw cell, which is well documented in the literature.[1–3] Transport in porous media has a wide variety of applications in oil industry, chemical processing, hydrology *etc.* This instability occurs when flows with variable mobility are involved.[3,4] The pattern formed due to the instability at the evolving interfaces of two miscible[5,6] or immiscible[2] fluids has been studied by various techniques. VF is, among others, also important in liquid chromatography, a flow based separation method. In this technique, a given fluid (called displacing fluid) displaces a miscible sample consisting of a solvent in which a mixture of solutes (also named analytes) is dissolved. The solutes are separated during the displacement because of selective adsorption on the porous matrix and/or selective transport properties. The fluid flow in a porous medium plays an important role in these separation techniques. Indeed, if the sample solvent has a different viscosity than that of the displacing fluid, VF can come into play, leading to distortion and widening of output peaks in the fingering zone.[7,8] Moreover, the strength of the adsorption on the porous matrix depends on the local fluid composition and can depend on the concentration of the sample solvent. Such an effect is called the solvent strength effect and it can interplay with viscous fingering as this hydrodynamic instability will lead to fingering of the solvent and hence to non trivial spatio-temporal changes in the adsorption rate. Similar coupling between fingering effects and adsorption on the porous matrix varying with the local composition of the fluids can be encountered in environmental issues as well like in $CO_2$ sequestration for instance.

In this context, it is the objective of this work to develop a generalized model to study theoretically how the transport of a solute in a porous media can be affected by the interplay of both VF and solvent strength effects. Despite a great deal of

[a]*Department of Mathematics, Indian Institute of Technology Ropar, 140001 Rupnagar, India. E-mail: manoranjan@iitrpr.ac.in*

[b]*Nonlinear Physical Chemistry Unit, Service de Chimie Physique et Biologie Théorique, Université Libre de Bruxelles (ULB), CP 231, 1050 Brussels, Belgium*

[c]*Ecole Supérieure de Physique et de Chimie Industrielles, Laboratoire de Physique et Mécanique des Milieux Hétérogènes, PMMH, UMR, 7636 CNRS, ESPCI-ParisTech - Université Pierre et Marie Curie - Université Paris-Diderot, 10, rue Vauquelin, 75231 Paris Cedex 05, France*

experimental work done in the field of chromatography, there is so far no theoretical study of such combined physico-chemical effects of VF and solvent strength to understand the separation of solutes undergoing variable sorption in a chromatographic column. This phenomenon is also largely unexplored in environmental applications.

Before explaining our model, let us first review what is known so far in this field in chromatography. On one hand, VF has been found to be detrimental for the separation of solutes in various high performance liquid chromatographic (HPLC) separation techniques like Reverse Phase Liquid Chromatography (RPLC) or Size Exclusion Chromatography (SEC) because it leads to distortion and widening of output peaks as shown experimentally.[9–12] In chromatography the focus is on a finite width sample of a given viscosity being displaced by a fluid of different viscosity. Viscous fingering develops on either the frontal or rear interface of the sample depending where the less viscous fluid displaces the more viscous one, the other interface being stable.[13–15] VF is also only a transient phenomenon since dispersion of the finite sample and mixing due to VF reduce the viscosity gradient in the course of time. A numerical study of VF effects in RPLC conditions has confirmed that, if the injection solvent is more viscous than the displacing fluid, the rear interface shows distortions.[16] The quantitative comparison of the influence of such VF on the peaks shows that, for a given viscosity ratio, the peak broadening is larger when the sample solvent is less viscous than the displacing fluid than in the opposite case.[17]

Another specificity important for VF in chromatography is that, besides being entrained by the flow, the solutes or analytes can also be retained on the stationary phase of the column. In that regard, a reduction of VF effects has been observed experimentally in case of an increase in retention of the solute.[8,15,18] To describe this situation, a three-component system has been modelled mathematically considering the solute as a passive scalar, its spatio-temporal dynamics being affected by VF of the sample solvent, when this solvent in more[19] or less[20] viscous than the displacing fluid. It was shown that the dynamics of the solute is affected not only by VF of the sample solvent but also by retention of the solute on the porous matrix.

On the other hand, another physico-chemical effect which leads to distortions of the peak profile of the solute independently of VF is the solvent strength effect which occurs when the displacing fluid has a weaker solvent strength than the sample solvent, *i.e.* a lower ability to displace the solutes from a particular stationary phase. Then, the retention factor $k$ of the solute on the porous matrix depends on the local concentration $c$ of the sample solvent. The deformation of the solute zone occurs because of the different migration velocities of the frontal and rear part of this zone. In such a situation, Jandera and Guiochon[21] have observed, in RPLC, a deformation and even a splitting of the band profiles. Such a peak splitting phenomenon has been simulated by Ng and Ng[22] using a model in which the retention factor is changed as the sample solvent moved through the column.

A dependence of the retention factor on the carrier liquid composition is generally occurring in comprehensive two-dimensional liquid chromatography (2D-LC). In 2D-LC, sample component fractions collected from the exit of a first column are injected in a second chromatographic column and displaced with a carrier liquid of a different nature or composition from that of the first column. Such a difference may give rise to a solvent strength effect as well as, when it is associated to a viscosity difference, to a VF effect. The magnitude of these two effects depends strongly on the sample volume. Understanding their influence on dispersion of the solute is essential for the optimization of the 2D-LC process since the fraction collection volume is a key parameter to be optimized.

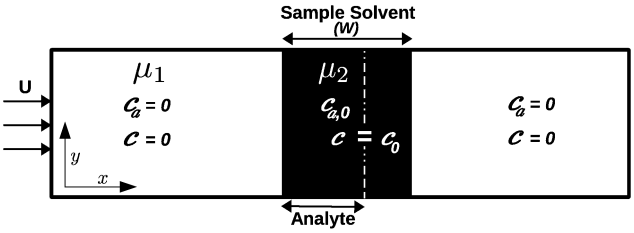


Fig. 1 Sketch of the system.

Recently, the contribution of the solvent strength effect in pure dispersive sample solvent case has been discussed by Mishra *et al.*[23] The band peaks have been found to be non-Gaussian even in the absence of VF because of the solvent strength effect. The peak distribution is bimodal leading to broadening of band and becomes unimodal only after disengagement of the solute from the sample solvent which matches well with experimental results.

In order to understand the combined effect of VF and solvent strength on the peak profiles, we develop here a mathematical model for the displacement of a sample of given viscosity by a displacing fluid of different viscosity combined to a solvent strength effect *i.e.* a concentration dependent retention $k(c)$ on the porous matrix of the solute controlling the viscosity. The model equations lead to fully coupled non-linear partial differential equations of convection–diffusion type for the solute and the sample solvent. The flow velocity in the porous column is modeled with Darcy's law. In order to analyze the evolution and distribution of the solute and sample solvent a numerical study has been performed. We find that the physico-chemical phenomena *i.e.* viscous instability and the solvent strength effect occur simultaneously, leading to a complex dynamical pattern by partially canceling each other. A critical analysis of the deformation of the solute peaks is done by calculating the second central moment or the variance which measures the spread of the peak.

## 2 Physical problem and governing equations

Our model system is a two-dimensional porous medium, in which a sample of length $W$ with a solvent concentration $c = c_0$ and of viscosity $\mu_2$ is injected at an initial time (see Fig. 1). The sample contains the solute in concentration $c_a = c_{a,0}$. It is confined between two regions filled by another miscible fluid, the displacing fluid, of viscosity $\mu_1$ ($\mu_1 < \mu_2$). The concentrations

 

of the solute and of the sample solvent inside the displacing fluid are $c_a = 0$ and $c = 0$ respectively.

Once the sample is injected in the system, the solute starts to be adsorbed on the porous matrix. We assume that this adsorption process is characterized by a linear isotherm dependence between the concentrations of the solute in the mobile phase $c_{a,m}$ and in the stationary phase $c_{a,s}$ as $c_{a,s} = Kc_{a,m}$ where $K = k_a/k_d$ is the equilibrium constant with $k_a$ and $k_d$ being the adsorption and desorption kinetic constants. The retention of the solute is characterized by the retention factor $k = FK$, where $F = V_s/V_m$ is the ratio between the volume of the stationary phase $V_s$ and the volume of the mobile phase $V_m$.

In the following, we consider that the solute retention mechanism is that prevailing in RPLC, the most commonly used mode of retention in liquid chromatography. In this mode, the displacing fluid is generally a mixture of water and of an organic modifier (which in most cases is methanol (MeOH) or acetonitrile (ACN)) with a volume fraction $\phi_m$ in organic modifier. The sample solvent is a mixture of water with that organic modifier having a volume fraction $\phi_s \geq \phi_m$. Since the displacing fluid and the sample solvent have different solvent strength the solute retention depends upon the composition of the sample solvent *i.e.* $k = k(c)$. As explained in Snyder *et al.*,[24] as a first approximation this concentration dependence of $k$ can be deduced from the relation $\ln k = \ln k_0 - S\phi$ where $k_0$ is the retention factor of the solute in pure water, $\phi$ is the volume fraction of the organic modifier and $S = 2.3S'$, where $S'$ is the solvent strength parameter. $S'$ has a value of about 3, which means that $k$ in pure MeOH or pure ACN is about 1000 times smaller than in pure water. The normalized composition of the liquid phase is $c = \dfrac{\phi - \phi_m}{\phi_s - \phi_m}$, hence the initial concentration of the sample solvent is $c_0 = 1$. Simplifying the above relation as in Mishra *et al.*,[23] the dependence of the retention factor on the concentration of the sample solvent reduces to

$$k(c) = k_m e^{-S^* c}, \tag{1}$$

with $S^* = \ln(k_m/k_s)$ where $k_m$, $k_s > 0$ are the retention parameters in the mobile phase and in the pure sample solvent, respectively.

Eqn (1) expresses the fact that the retention factor $k$ is equal to $k_m$ in absence of the solvent of the sample ($c = 0$) and has a value that decreases with $c$ in the mixture of injected fluid and displaced sample solvent. The retention factor increases thus when the solute leaves the sample solvent to go to the displacing fluid. Other functions than eqn (1) can be chosen but this one is validated by a large number of experimental data in RPLC.

The fluids are displaced uniformly with a mean velocity $U$ along the $x$-direction. Because the solute is retained, at the end of the injection process, *i.e.* at the time $t = 0$, the length occupied by the solute zone is different from that of the sample solvent zone. We assume that, at time $t = 0$, these two slices have a rectangular shape and the rear boundaries of both zones are at the same position. Hence the length of the solute zone is smaller and equal to $W/(1 + k_s)$. Here the retention value of the solute is selected as $k_s$ since the solute is surrounded by the pure sample solvent.

The viscosity is assumed to depend upon the concentration $c$ of the sample solvent only, through an exponential relation of Arrhenius type[5,19] $\mu(c) = \mu_1 e^{Rc}$, where $R$ is the log mobility ratio defined as $R = \ln(\mu_2/\mu_1)$. With $\mu_2 > \mu_1$, $R > 0$, hence the rear interface of the sample solvent shows viscous fingering. As soon as $R \neq 0$ and $S^* \neq 0$, both VF and solvent strength effects are operational. In that case, the spatio-temporal evolution of the concentration of the solute will be influenced by both the deformation of the sample solvent zone by VF and by the adsorption of the solute on the porous matrix.

Assuming the fluid to be incompressible and velocity to be governed by Darcy's law inside the porous medium,[3,25] the evolution equations in vector form become,[19]

$$\underline{\nabla} \cdot \underline{u} = 0, \tag{2}$$

$$\underline{\nabla} p = -\frac{\mu(c)}{K_p}\,\underline{u}, \tag{3}$$

$$\frac{\partial c}{\partial t} + (\underline{u} \,.\, \underline{\nabla})c = D_x \frac{\partial^2 c}{\partial x^2} + D_y \frac{\partial^2 c}{\partial y^2}, \tag{4}$$

$$\frac{\partial c_{a,m}}{\partial t} + F\frac{\partial c_{a,s}}{\partial t} + \underline{u} \,.\, \underline{\nabla}\, c_{a,m} = D_{a,x} \frac{\partial^2 c_{a,m}}{\partial x^2} + D_{a,y} \frac{\partial^2 c_{a,m}}{\partial y^2}, \tag{5}$$

where $\underline{\nabla} = \left(\dfrac{\partial}{\partial x}, \dfrac{\partial}{\partial y}\right)$, $K_p$ is the permeability of the porous medium, $p$ is the pressure and $\underline{u} = (u, v)$ is the two-dimensional velocity vector, with $u$ and $v$ the velocity component in $x$ and $y$ direction, respectively. Eqn (4) is the convection–diffusion equation for the concentration $c$ of the sample solvent ruling the viscosity of the solution, where $D_x$, $D_y$ are its dispersion coefficients in the $x$ and $y$ direction respectively. Eqn (5) is the mass balance equation, with both mobile $c_{a,m}$ and stationary phase $c_{a,s}$ components of the solute concentration $c_a$ where $F = V_s/V_m$ is the phase ratio of the volumes in stationary phase $V_s$ and mobile phase $V_m$ respectively.[11] $D_{a,x}$ and $D_{a,y}$ are the dispersion coefficients of the solute along $x$ and $y$ directions. All previous works done on separated VF or solvent strength effects can be recovered as particular cases of this very general system of equations. In the particular case of uniform flow and viscosity independent of the sample solvent concentration ($R = 0$), we get the equations studied by Mishra *et al.*[23] for the pure solvent effect. By taking $S^* = 0$ in the present model, the VF results of Mishra *et al.*[19] with a constant retention factor can be retraced. If $k_m$ is also taken equal to 0, we get back to VF with no adsorption as analysed by De Wit *et al.*[14] *i.e.* the two component model. The boundary conditions are:

$$u = U,\ v = 0 \text{ and } \frac{\partial c}{\partial x}, \frac{\partial c_{a,m}}{\partial x} = 0, \quad \text{at the inlet and outlet} \tag{6}$$

$$\frac{\partial v}{\partial y} = 0, \frac{\partial c}{\partial y} = 0, \frac{\partial c_{a,m}}{\partial y} = 0, \forall x \quad \text{at the transverse boundaries} \tag{7}$$

As explained in Mishra *et al.*,[19] the mobile phase concentration $c_{a,m}$ of the solute varies from 0 in the pure displacing fluid to $c_{a,0}$ in the sample solvent. To non-dimensionalize the governing equations, we take $c_{a,0}$ as the reference concentration

for the solute, $U$ as the characteristic velocity, the length scale as $L_c = D_x/U$ and a time scale as $t_c = D_x/U^2$. The non dimensional quantities are then obtained as

$$\hat{x} = \frac{x}{L_c},\ \hat{y} = \frac{y}{L_c},\ \hat{t} = \frac{t}{t_c},\ \hat{u} = \frac{u}{U},\ \hat{v} = \frac{v}{U},$$

$$p^* = \frac{p}{\mu_1 D_x/K_p},\ \mu^* = \frac{\mu}{\mu_1},\ c^*_{a,m} = \frac{c_{a,m}}{c_{a,0}},\ \varepsilon = \frac{D_y}{D_x},$$
$$\varepsilon_a = \frac{D_{a,y}}{D_{a,x}},\ \delta = \frac{D_{a,x}}{D_x}$$

We further introduce a reference frame moving with the flow velocity, $x^* = \hat{x} - \hat{t}$, $y^* = \hat{y}$, $u^* = \hat{u} - 1$, $v^* = \hat{v}$, $t^* = \hat{t}$. Using the linear isotherm adsorption hypothesis, the non dimensional form of the governing eqn (2)–(5) along with the viscosity relation $\mu(c)$ and retention relation $k(c)$ (as in eqn (1)) become after dropping the superscripts (*):

$$\underline{\nabla}\cdot\underline{u} = 0, \tag{8}$$

$$\underline{\nabla}p = -\mu(c)(\underline{u} + \underline{e}_x), \tag{9}$$

$$\frac{\partial c}{\partial t} + \underline{u}.\underline{\nabla}c = \frac{\partial^2 c}{\partial x^2} + \varepsilon\frac{\partial^2 c}{\partial y^2}, \tag{10}$$

$$\frac{\partial c_{a,m}(1+k(c))}{\partial t} + u\frac{\partial c_{a,m}}{\partial x} - \frac{\partial c_{a,m}(k(c))}{\partial x} + v\frac{\partial c_{a,m}}{\partial y} = \delta\left[\frac{\partial^2 c_{a,m}}{\partial x^2} + \varepsilon_a\frac{\partial^2 c_{a,m}}{\partial y^2}\right], \tag{11}$$

$$\mu(c) = e^{Rc}, \tag{12}$$

$$k(c) = k_m e^{-S^* c}, \tag{13}$$

where $\underline{e}_x$ is the unit vector along the $x$-direction. With the above dimensionless scales, the non-dimensional length and width of the domain are $L' = UL_x/D_x$, and a Péclet number $Pe = UL_y/D_x$, where $L_x$ and $L_y$ are their dimensional measures, respectively. Hence the non-dimensionalised boundary conditions in the moving frame along the inlet and outlet boundaries (eqn (6)) reduce to

$$u = 0,\ v = 0,\ \frac{\partial c}{\partial x}, \frac{\partial c_{a,m}}{\partial x} = 0, \tag{14}$$

and along the transverse boundaries, without loss of generality, the boundary conditions of eqn (7) can be considered equivalent to periodic boundary conditions as:

$$u(x, 0, t) = u(x, Pe, t),\ (c, c_{a,m})(x, 0, t) = (c, c_{a,m})(x, Pe, t). \tag{15}$$

In order to numerically solve the system of eqn (8)–(15), we use a stream-function formulation to reduce the number of variables and because the stream function has been observed to be a more convenient and independent variable than the pressure field or velocity field.[5,6] Moreover, for distorted interfaces there is a significant reduction in computation time of the stream function in comparison to that of the velocity field. Hence introducing the stream function $\psi(x, y)$ as $(u, v) = (\partial\psi/\partial y, -\partial\psi/\partial x)$. The governing eqn (8)–(13) become

$$-\nabla^2\psi = R\left(\frac{\partial\psi}{\partial x}\frac{\partial c}{\partial x} + \frac{\partial\psi}{\partial y}\frac{\partial c}{\partial y} + \frac{\partial c}{\partial y}\right), \tag{16}$$

$$\frac{\partial c}{\partial t} + \frac{\partial\psi}{\partial y}\frac{\partial c}{\partial x} - \frac{\partial\psi}{\partial x}\frac{\partial c}{\partial y} = \frac{\partial^2 c}{\partial x^2} + \varepsilon\frac{\partial^2 c}{\partial y^2}, \tag{17}$$

$$\frac{\partial c_{a,m}(1+k(c))}{\partial t} - \frac{\partial c_{a,m}k(c)}{\partial x} + \frac{\partial\psi}{\partial y}\frac{\partial c_{a,m}}{\partial x} - \frac{\partial\psi}{\partial x}\frac{\partial c_{a,m}}{\partial y} = \delta\left[\frac{\partial^2 c_{a,m}}{\partial x^2} + \varepsilon_a\frac{\partial^2 c_{a,m}}{\partial y^2}\right]. \tag{18}$$

It is clear from above that eqn (18) is decoupled from eqn (16) and (17). Hence once the stream function $\psi$ and the solvent concentration $c$ are evaluated from eqn (16) and (17) for a given $R$, the transport of the solute concentration $c_{a,m}$ can be determined from eqn (18) for different values of the solute parameters ($k_m$, $S^*$, $\delta$, $\varepsilon_a$).

### 2.1 Numerical method

Eqn (16)–(18) are solved numerically using a Fourier pseudo-spectral technique.[26] In this technique the variables $c$, $c_{a,m}$ and $\psi$ are evaluated in the Fourier space in order to compute the spatial derivatives and the evolution of the concentration fields in time. The non-linear and variable coefficient terms are calculated in the real physical space. The concentration fields and the other variables are represented as Fourier series as,

$$c(x, y, t) = \sum_p\sum_r \hat{c}_{p,r}(t)e^{i(k_p x + k_r y)}, \tag{19}$$

with $i^2 = -1$ and where $\hat{c}$ are the Fourier coefficients of $c$ calculated at discretized collocation points, $k_p$ and $k_r$ are the wave numbers of the Fourier modes. The Fourier discretization is uniform in space and is truncated at $p = 0$ and $p = M - 1$, $r = 0$ and $r = N - 1$, where $M$ and $N$ are the grid point numbers in the $x$ and $y$ directions, respectively. The transformation between the real and the Fourier space is done by using fast Fourier transformation with the order of complexity $\mathbf{N}\log_2\mathbf{N}$, where $\mathbf{N} = M \times N$. Eqn (16) and (17) are classical miscible VF equations already studied at length since Tan and Homsy.[5] Eqn (18) is a non-linear partial differential equation with variable coefficients.

The Fourier representation of the non-linear and variable coefficient terms in eqn (18) is:

$$J_1(x, y, t) = \frac{1}{(1+k(c))}\left(\delta\left[\frac{\partial^2 c_{a,m}}{\partial x^2} + \varepsilon_a\frac{\partial^2 c_{a,m}}{\partial y^2}\right] - \left(\frac{\partial\psi}{\partial y}\frac{\partial c_{a,m}}{\partial x} - \frac{\partial\psi}{\partial x}\frac{\partial c_{a,m}}{\partial y}\right) + k(c)\frac{\partial c_{a,m}}{\partial x} + S^*k(c)c_{a,m}\left[\frac{\partial^2 c}{\partial x^2} + \frac{\partial^2 c}{\partial y^2} - J(x, y, t) - \frac{\partial c}{\partial x}\right]\right) = \sum_p\sum_r \hat{J}_{1_{p,r}}(t)e^{i(k_p x + k_r y)}. \tag{20}$$

With the above representation, the equations in Fourier space become a system of algebraic differential equations:

$$\hat{\psi}_{p,r} = R(\hat{N}_{p,r} + \mathrm{i}k_r\hat{c}_{p,r})/(k_p{}^2 + k_r{}^2), \quad (21)$$

$$\frac{\mathrm{d}\hat{c}_{p,r}}{\mathrm{d}t} = -\hat{J}_{p,r} - \left(k_p{}^2 + k_r{}^2\right)\hat{c}_{p,r}, \quad (22)$$

$$\frac{\mathrm{d}\hat{c}_{1_{p,r}}}{\mathrm{d}t} = \hat{J}_{1_{p,r}}, \quad (23)$$

where $\hat{N}, \hat{J}$ are the Fourier coefficients of the non-linear terms in eqn (16) and (17) respectively (*cf.* Tan and Homsy[5]). The terms $\hat{N}$, $\hat{J}$ and $\hat{J}_1$ are evaluated pseudo-spectrally by transforming variables $\hat{c}$, $\hat{\psi}$ and $\hat{c}_1$ to real physical space, computing all the terms having non-linear and variable coefficients in the same real physical space and then transforming back to Fourier space.

The time-stepping scheme used is a predictor-corrector method, with a second order Adams–Bashforth scheme for predicting the variables which are corrected by using a trapezoidal rule. A similar algorithm has been followed by Mishra *et al.*[23] for eqn (23) and by Tan and Homsy[5] for eqn (21) and (22). The spectral method used to solve the system of partial differential equations is more accurate on a coarser discretization grid of the spatial domain in comparison to other numerical methods like finite differences or finite elements. Hence it is advantageous to use this method as it requires lesser memory while achieving a higher accuracy. Moreover, there is no or very little numerical dissipation with spectral methods.[27]

As initial condition, the non-dimensional initial length of the sample solvent zone is $l = UW/D_x$ with $x = 0$ as the middle of the sample solvent zone. So the initial non-dimensionalised length of the solute zone is $l_a = l/(1 + k_s)$.[23] The rear boundary of both the solute and the sample solvent zones are at the same position $x = -l/2$. So, the frontal boundary of the solute will be at $x = \dfrac{l(1-k_s)}{2(1+k_s)}$ and that of the sample solvent at $x = l/2$. The initial conditions for the sample solvent and the solute concentrations correspond to a rectangular sample of concentration $c = 1$, $c_{a,m} = 1$ and of size Pe $\times$ $l$ and Pe $\times$ $l_a$ respectively in a $c = c_{a,m} = 0$ background. To apply the Fourier pseudo-spectral method, periodic boundary conditions are employed along the longitudinal and transverse directions. Our simulations were performed on a rectangular domain $L' \times$ Pe discretized using a lattice of 8192 $\times$ 128 grid points.

## 3 Results and discussion

In the porous medium, the solute undergoes both a linear adsorption in the mixture of displacing fluid and sample solvent with a strong solvent strength and the influence of VF occurring between these two fluids. The resulting dynamics of the solute is studied here in the case of a positive log-mobility ratio $R$, *i.e.* a less viscous displacing fluid displacing the sample solvent with a solute retention factor $k$ depending locally on $c$, as given by eqn (13). In this generalized model, when $k_m = 0$, $\delta = 1$ and $\varepsilon_a = \varepsilon$ we obtain the two component system,[14] so the evolution profile of the solute is the same as that of the sample solvent as shown in Fig. 2a. This fingering dynamics of the sample solvent affects the evolution of the solute concentration

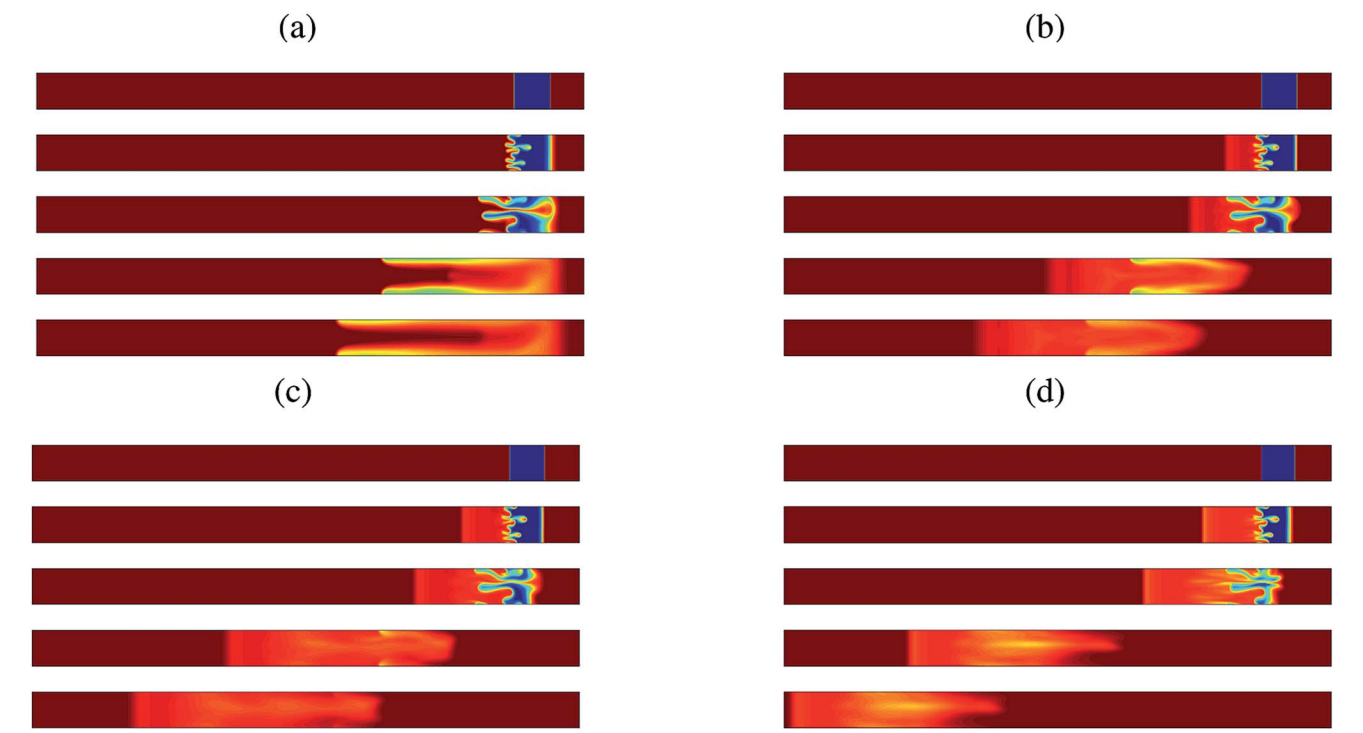


Fig. 2 Evolution of the local solute concentration $c_a$ with $l = 512$, $\varepsilon = 1$, $\varepsilon_a = 1$, $\delta = 1$, $R = 2$ and $S^* = 4$ for (a) $k_m = 0$, (b) $k_m = 1$, (c) $k_m = 2$ and (d) $k_m = 5$ at $t = 0$, 1000, 2000, 6000 and 8000 from top to bottom.

in two ways. Firstly it affects the retention of the solute on the stationary phase (see eqn (5)). Secondly the solute zone develops fingers when either of its interface comes in contact with the unstable interface of the sample solvent. The combined effect of these two perturbations, VF and the solvent strength effect, on the evolution of the solute is analysed for different values of the parameters $k_m$, $S^*$ and $R$ chosen to maximize the effect on the solute distribution.

### 3.1 Effect of retention parameter $k_m$

Since at any instant the solute is present in both stationary and mobile phases, its evolution is tracked by following its local overall concentration, $c_a(x, y, t)$ which, according to eqn (11) is proportional to $(1 + k(c))c_{a,m}$. The dynamics of $c_a$ is shown in Fig. 2 at successive times for different values of $k_m$ by fixing $S^* = 4$, $l = 512$ and $R = 2$. The parameter values are taken to match the typical experimental situations encountered in analytical HPLC column. For instance in a 4.6 mm i.d. HPLC column packed with 3 μm particles with a total porosity 0.7 and solute with a reduced plate height of 3, the sample length $l = 512$ considered in this study corresponds to an injection volume of 27 μL. The value 4 is selected for $S^*$, corresponding to $S' = 3$ and to $(\phi_s - \phi_m) = 0.6$ characteristic of organic solvent–water mixtures.

Fig. 2a shows the evolution of the solute zone with $k_m = 0$ *i.e.* in absence of adsorption. In this case VF is observed at the rear of the sample (*i.e.* the left region of the solute zone) where the less viscous fluid displaces the more viscous one. The frontal interface of the sample solvent being stable undergoes pure diffusion. The solute zone is advected by the resulting flow and follows the same dynamics as that of the sample solvent. Hence the three component system is reduced to the two component system which has already been studied by De Wit *et al.*[14] In Fig. 2b–d the evolution of $c_a$ with $k_m = 1$, 2 and 5 is shown for successive times. The solute is observed to develop two separated significant concentration zones, one inside the sample solvent as seen by the solute fingers which are affected by VF (referred to as the locked-in region). The second one is dragged along the displacing fluid (referred to as the dragged-along region) and features a dispersive regime outside the solvent affected zone. The dragged-along region of solute appears behind the rear of the locked-in region and moves away from the sample solvent as time $t$ is increased. It is observed that the dragged-along region of solute dilutes with time into the bulk of the displacing fluid. After a while both interfaces of the locked-in region start interacting and the time of this interaction arises earlier for larger values of $k_m$. The extent of the fingering pattern in the locked-in region is found to reduce with an increase of the retention parameter in the mobile phase $k_m$. This is because the solute zone is locked for lesser time inside the sample solvent for larger values of $k_m$. Hence it comes out faster from the solvent zone thus is less affected by VF. Since we are in a frame of reference moving with the injection velocity, the sample solvent has no bulk motion and the solute zone has an axial advection velocity in the upstream direction (towards the left in the figures). Hence we say that the solute zone comes out of the sample solvent zone faster so that it is more retained by adsorption on the stationary phase. A similar analysis can also be done in the laboratory frame of reference, where both the sample solvent and the solute zones move in the downstream direction with the sample solvent moving at a higher velocity than the solute zone. So the solute region lags behind the sample solvent zone and disengages from the sample solvent.

As can be seen from Fig. 2b–d the solute zone is inside the sample solvent area for $k_m = 1$, 2 till $t \simeq 8000$ whereas for $k_m = 5$ it is outside the sample solvent zone at that time. Hence, the solute is less affected by VF for $k_m = 5$ as compared to smaller values of the retention parameter $k_m$.

A quantitative analysis of the evolution of the solute concentration is done by plotting the transversed average profile of the solute concentration in mobile phase $\bar{c}_{a,m}$ and the local cross sectional average solute mass, $\bar{c}_a$, defined as[14]

$$\bar{c}_{a,m}(x,t) = \frac{1}{Pe}\int_0^{Pe} c_{a,m}(x,y,t)\mathrm{d}y, \tag{24}$$

$$\bar{c}_a(x,t) = \frac{1}{Pe}\int_0^{Pe} (1 + k(c))c_{a,m}(x,y,t)\mathrm{d}y. \tag{25}$$

These quantities are computed at successive times for the fixed values $k_m = 5$, $S^* = 4$ and $R = 2$. The detectors in chromatograms give similar plots. The set of eqn (16)–(18) are solved for the concentration of the sample solvent and solute mass in the mobile phase $c_{a,m}$. Thus to study their peak distribution along the migration axis the transverse average concentration profile of the sample solvent $\bar{c}(x, t)$ and of the solute in the mobile phase $\bar{c}_{a,m}(x, t)$ are plotted. Fig. 3a shows the average concentration $\bar{c}(x, t)$ of the sample solvent (*i.e.* $\bar{c} = \frac{1}{Pe}\int_0^{Pe} c(x,y,t)\mathrm{d}y$) or $\bar{c}_{a,m}$ with $k_m = 0$ which corresponds to Fig. 2a. The concentration profile shows distortions due to fingering. Such distorted peaks are observed experimentally also in RPLC.[7,8,11] $\bar{c}_{a,m}(x, t)$ is shown in Fig. 3b at different times. Similarly, inside the sample solvent, $\bar{c}_{a,m}(x, t)$ is affected by VF and hence its profile also gets distorted. The downstream distribution peak of $\bar{c}_{a,m}(x, t)$ advects with a velocity $k_m/(1 + k_m)$ in the axial direction, which leads to a larger spreading of the solute.

Fig. 3c shows the local cross sectional average solute concentration $\bar{c}_a$ corresponding to Fig. 2d. The rear interface is affected by VF with a stable frontal interface as $R > 0$. The area of the distribution of the solute is constant in time. This confirms the conservation of the solute mass $\bar{c}_a$ (see Fig. 3c) unlike the quantity $\bar{c}_{a,m}$ (see Fig. 3b). The VF of the sample solvent affects the dispersion dynamics of the solute and thus fingering effects are seen in the average solute concentration profiles $\bar{c}_a(x, t)$. The upstream distribution profile corresponds to the solute zone dragged along the displacing fluid as seen in the density plots of the solute (Fig. 2). It features a standard error function which is a characteristic of a pure dispersion profile for the corresponding parameters in Fig. 3c. The appearance of this left peak tail is due to the effect of the solvent strength parameter $S^*$, which leads to variable advection and diffusion speed of the solute that comes out of the

 

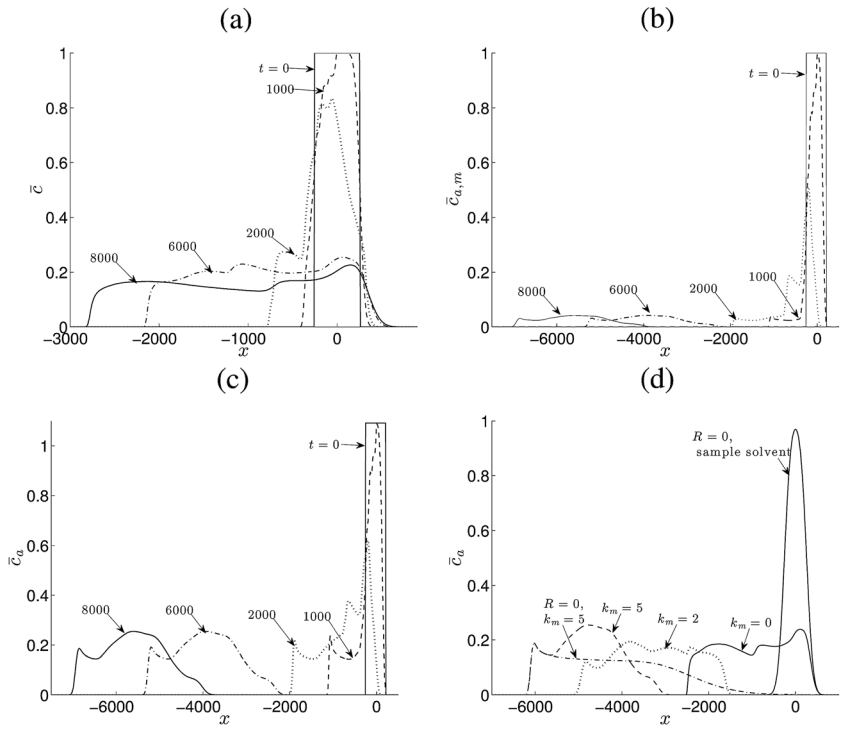


Fig. 3 (a) Cross-sectional average concentration profiles of the sample solvent $\bar{c}(x, t)$ as a function of $x$ for different times. (b) Average concentration profiles of the solute in the mobile phase $\bar{c}_{a,m}$ for different times with $k_m = 5$. Cross-sectional average solute concentration profiles $\bar{c}_a$ as a function of $x$, (c) for different times with $k_m = 5$, and (d) for different values of $k_m$ at $t = 7000$. Other parameters have the same value as in Fig. 2.

sample solvent.[23] For $R > 0$, the VF dynamics of the sample solvent zone affects the solute retention in it, thus distortions are seen on the concentration peak of the solute locked inside the sample solvent. Both interfaces of the solute zone can then be affected by VF depending on when they come in contact with the VF of the sample solvent. Further in time, the solute

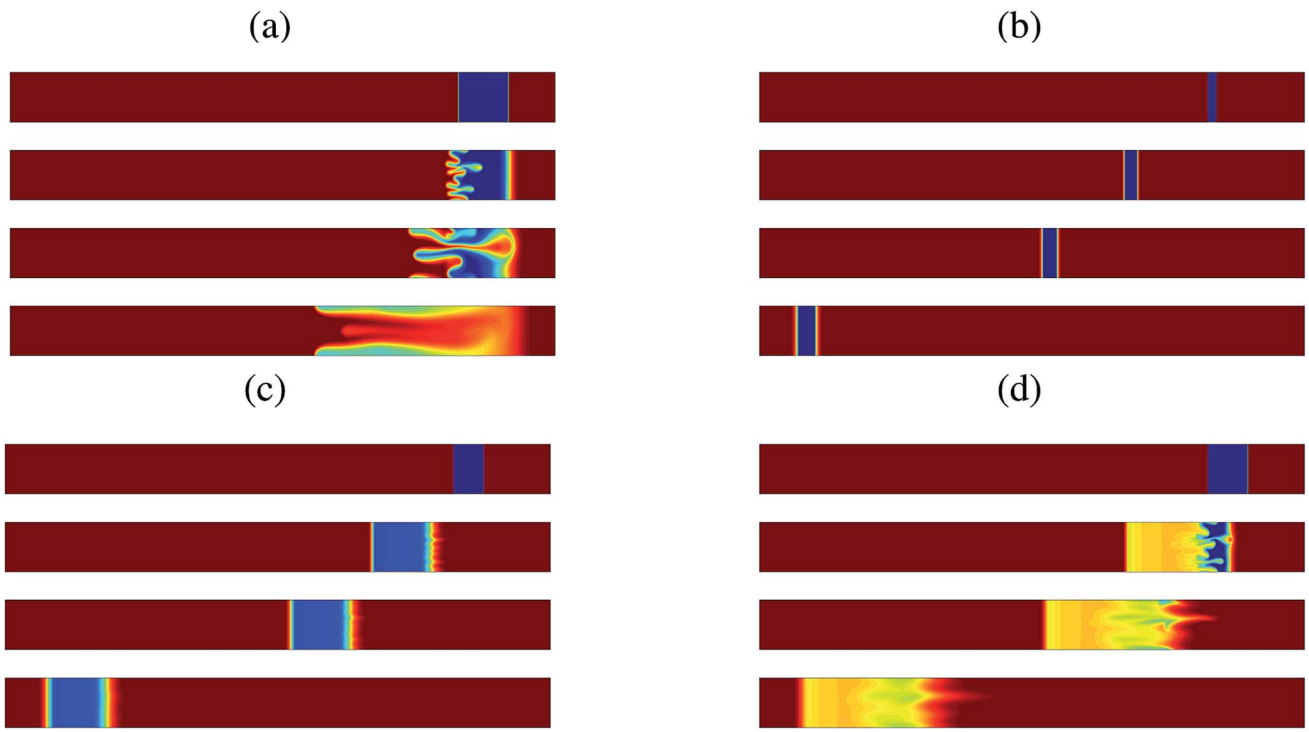


Fig. 4 (a) Evolution of the concentration of the sample solvent $c$. Local solute concentration $c_a$ with $l = 512$, $\varepsilon = 1$, $\varepsilon_a = 1$, $\delta = 1$, $R = 2$ and $k_m = 5$ for (b) $S^* = 0$, (c) $S^* = 2$ and (d) $S^* = 3$ at $t = 0$, 1000, 2000 and 5000 from top to bottom.

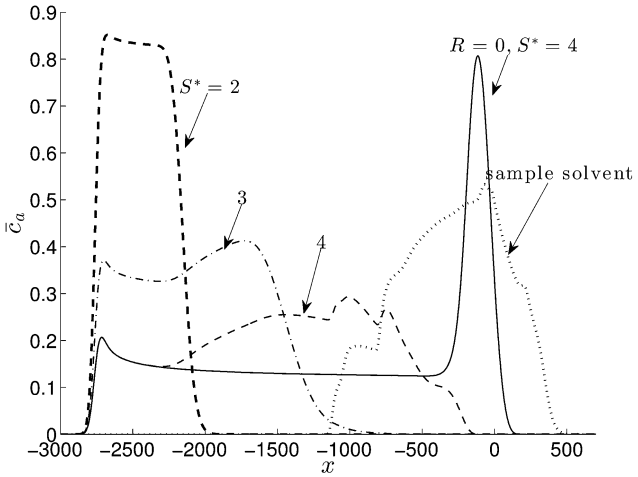


Fig. 5 Cross-sectional average concentration profile of the solute $\bar{c}_a(x, t)$ as a function of $x$ for different values of the solvent strength parameter $S^*$ at $t = 3000$ with $R = 2$, $k_m = 5$, $l = 512$, $\varepsilon = 1$, $\varepsilon_a = 1$, $\delta = 1$.

comes out of the sample solvent and thus goes out of the VF affected zone. It is clearly seen from Fig. 3a and b at $t \simeq 8000$ that the frontal interface of the solute is at $x \simeq -3900$ whereas the rear interface of solvent is at $x \simeq -2700$, so the solute zone is completely disengaged from the sample solvent zone. The spreading zone of the solute has also been reduced due to adsorption of the solute on the porous matrix.

In order to further quantify the influence of $k_m$ on the peak profiles of $c_a$, we plot in Fig. 3d, the average concentration of the solute $\bar{c}_a$ for different values of $k_m$ at time $t = 7000$. The left tail of the solute distribution, which corresponds to the pure dispersion profile of the solute zone dragged along the displacing fluid unaffected by VF, moves further away from the sample solvent zone with increasing values of the retention parameter $k_m$. But the remaining solute profile remains under the effect of VF, thus showing distorted peak shapes. The non dimensional axial advection speed of the solute in the mobile phase in the upstream direction is $k(c)/(1 + k(c))$ in the moving frame of reference. As $c_a$ is proportional to $c_{a,m}$, it also propagates with a speed proportional to that of the solute in the mobile phase. With an increase in $k_m$, the advection speed of the solute increases in the upstream direction hence it moves out faster from the sample solvent. Also it is known that VF leads to a faster reduction of the sample solvent concentration. This leads to an increase in the effective retention $k(c)$ of the solute as it depends upon the local concentration of the sample solvent. Hence it ultimately increases the advection speed of the solute distribution in the upstream direction. This fact is clearly seen in Fig. 3d where for $k_m = 5$, $R = 0$, the distribution is advected to the left at a slower speed as compared to the distribution of the solute with $k_m = 5$, $R = 2$.

### 3.2 Solvent strength effects

Fig. 4 compares the dynamics of the sample solvent with that of the local average solute concentration $c_a$ for different values of the solvent strength parameters $S^* = 0$, 2, 3 which correspond to $\phi_s - \phi_m = 0\%$, 29%, 43% of the organic modifier (MeOH or ACN) with $S' = 3$ at fixed $k_m = 5$ and $R = 2$. Fig. 4a shows the evolution of the sample solvent and Fig. 4b depicts the

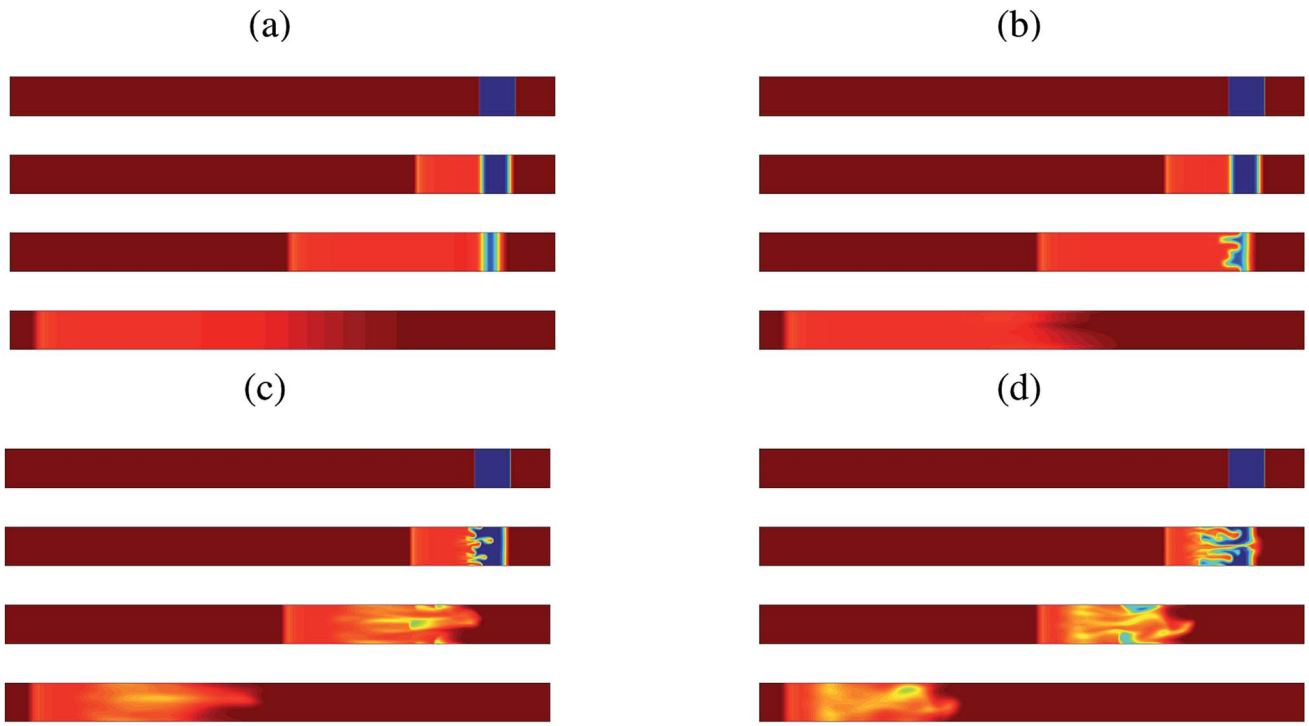


Fig. 6 Evolution of the local solute concentration $c_a$ with $l = 512$, $\varepsilon = 1$, $\varepsilon_a = 1$, $\delta = 1$, $S^* = 4$ and $k_m = 5$; for (a) $R = 0$, (b) $R = 1$, (c) $R = 2$ and (d) $R = 3$ at $t = 0$, 1000, 3000 and 7000 from top to bottom.

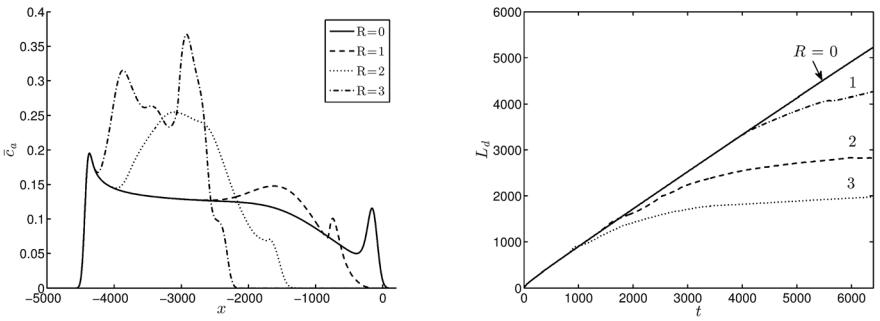


Fig. 7 Profile of the cross-sectional average solute concentration $\bar{c}_a(x, t)$ along the $x$-axis for different values of $R$ at $t = 5000$ with $S^* = 4$, $k_m = 5$, $l = 512$, $\varepsilon = 1$, $\varepsilon_a = 1$, $\delta = 1$. (b) Spreading length of the solute zone as a function of time for different values of $R$ with $k_m = 5$, $S^* = 4$, $l = 512$, $\varepsilon = 1$, $\varepsilon_a = 1$, $\delta = 1$.

evolution of the solute for $S^* = 0$ when the retention parameter is independent of the sample solvent concentration. Hence the solute zone moves with a uniform velocity whatever the fractional amount of the sample solvent in the displacing fluid.

With strong solvents $S^* \neq 0$, the dispersion dynamics of the solute changes from that for $S^* = 0$ [Fig. 4c and d]. Firstly, there is a change in the length of the solute zone as it depends now upon the sample solvent strength. The initial length of the solute zone $l_a = l/(1 + k_s)$ increases with an increase in $S^*$. Secondly, the spread of the solute zone increases with an increase in $S^*$. $S^* > 0$ implies that the solvent strength of the sample solvent is larger than that of the liquid phase ($\phi_s > \phi_m$), so the retention of the solute zone depends upon the local composition of the sample solvent. This leads to a variable velocity of the solute zone, the velocity being smaller for the part of the solute locked inside the sample solvent zone than for the part dragged along the displacing fluid.

Now for $S^* = 0$ the solute zone shows no fingering pattern as it comes out of the sample solvent before getting affected by VF. However with an increase in solvent strength $S^*$, the dragged-along region of solute develops outside the locked-in region. As mentioned earlier this dragged-along region of solute comes out of the sample solvent without interacting with its VF dynamics while the locked-in region interacts with the VF dynamics. There is an increase in disengagement time of the solute from the sample solvent. Thus distortions are seen for larger times for higher values of $S^*$. As can be seen in Fig. 4, at $t = 2000$ the solute zone is without fingering pattern for $S^* = 2$ (Fig. 4c) while fingering is still seen for $S^* = 3$ (Fig. 4d). Thus the presence of a strong sample solvent does affect the influence of VF on the solute zone.

The above result is quantitatively analysed by plotting the corresponding transversely averaged profiles $\bar{c}_a(x, t)$ for different values of $S^*$ in Fig. 5. The axial non dimensional advection speed of the solute in the upstream direction is proportional to $k(c)/(1 + k(c))$. It decreases with an increase in the solvent strength parameter $S^*$ and increases when the sample solvent concentration decreases along the $x$-axis. This is because of the dependence of the concentration $c$ on both $x$ and $t$. So the solute gets locked in for a larger time inside the sample solvent for increasing values of $S^*$. In Fig. 5 for $S^* = 2$ the solute is completely outside the sample solvent while for $S^* = 4$ it is still inside it. Hence the peak profile of the solute is more distorted for a larger solvent strength parameter $S^*$ (Fig. 4), whereas, because of a decrease in the concentration of the sample solvent in the liquid mixture due to VF, the advection speed of the locked-in solute zone increases. This can be clearly visualized in Fig. 5 by comparing the peak profile for $S^* = 4$ (that implies $\phi_s - \phi_m = 58\%$) with $R = 0$ and $R = 2$. It is seen that the locked-in part of the solute zone, advects faster for $R = 2$ than for $R = 0$. Hence the combined effect of VF and of the solvent strength effect significantly affects the flow dynamics of the solute.

### 3.3 Effects of log mobility ratio $R$

Since viscous fingering of the sample solvent due to $R \neq 0$ affects the solute distribution through adsorption and fingering dynamics, it is interesting to know how changing the viscosity contrast between the sample solvent and the displacing fluid, *i.e.* changing $R$, affects the evolution profile of the solute zone. For that purpose density plots of the solute concentration $c_a$ are plotted at successive times in Fig. 6 for different values of the log mobility ratio $R$ fixing $k_m = 5$ and $S^* = 4$. The concentration field of $c_a$ with $R = 0$ *i.e.* without VF is shown in Fig. 6a. It presents all the characteristics of the dynamics of $c_a$ in presence of a solvent effect as already studied by Mishra *et al.*[23] We know that, when $R > 0$, the rear interface of the sample solvent zone becomes unstable and shows VF, thereby displacing the centre of gravity of the sample solvent backwards with respect to the initial position. This fingering affects the dynamics of the local solute concentration as shown in Fig. 6b–d for different values of $R$. It is observed that, as the value of $R$ increases, fingering at the rear interface of the locked-in solute zone is observed earlier. The fingers travel faster for larger $R$ and hence the two interfaces of the locked-in solute zone interact faster for $R = 3$ as compared to lower values of $R$. The interesting fact is that the dragged-along solute zone has travelled the same distance irrespective of the increase in the viscosity contrast between the sample solvent and the displacing fluid.

We further investigate the effect of increasing the log mobility ratio on the profile of the cross sectional average solute

concentration (Fig. 7a). It is observed that for $R = 0$, the solute distribution profile becomes bimodal. This kind of bi-modality is seen is practice in RPLC conditions.[11,15,21,28] Further, it is observed that, with an increase in $R$, the upstream peak tail of the solute distribution is at the same position irrespective of the value of $R$. This is because as soon as the rear part of the solute zone comes out of the sample solvent, it advects with a constant speed $k_m/(1 + k_m)$. On the other hand, the concentration of the sample solvent decreases faster with an increase in $R$ thus increasing the effective retention of the solute. This in turn increases the advection speed of the locked-in solute zone, which travels faster with increasing $R$ and hence comes out of the sample solvent earlier. The disengagement time of the solute decreases with an increase in $R$ because of a faster mixing of the sample solvent. This leads to a decreased spreading of the solute. The effect of $R$ on the spreading of the solute can be analyzed by the dynamics of the mixing length $L_m$ shown in Fig. 7b. The mixing length is defined as $L_d = l_d - l_a$, where $l_d$ is the spreading length of the solute for the interval in which $\bar{c}_a(x, t) > 0.001$ and $l_a$ is the initial solute length.[19,20] As seen in Fig. 7b, the spreading length $L_d$ is largest for $R = 0$ and decreases with $R$. Fig. 6 also clearly depicts this decrease in the spreading length of the solute with increasing $R$. Hence, we conclude that VF of the sample solvent reduces the effect of the solvent strength on the solute propagation in the column. The band broadening of the solute only due to solvent strength effect[23] is reduced when combined with the VF effect of the sample solvent. In addition, the band broadening is reducing with an increase in viscosity contrast between the sample solvent and displacing fluid.

### 3.4 Variance of the solute

The present work models, among others, the flow separation dynamics in chromatography conditions. The solute plate height is one of the essential parameters to be considered by experimentalists in chromatography and it can be measured by the rate of change of the spatial variance of the solute zone in the column with respect to the distance along the column $x$. To analyse the effect of VF and adsorption on the solute plate height, we compute the second central moment, the variance $\sigma_a^2(t)$, from the cross-sectional average solute concentration profile as:[23]

$$\sigma_a^2(t) = \frac{\int_0^{L'} \bar{c}_a(x,t)[x - m(t)]^2 \mathrm{d}x}{\int_0^{L'} \bar{c}_a(x,t)\mathrm{d}x}, \quad (26)$$

where $m(t) = \int_0^{L'} xf(x,t)\mathrm{d}x$ is the first moment of $f(x, t)$, where

$$f(x,t) = \bar{c}_a(x,t) \Big/ \int_0^{L'} \bar{c}_a(x,t)\mathrm{d}x,$$

is the probability density function of the continuous distribution of the total solute mass $\bar{c}_a(x, t)$. The variance of the distribution when the solute is injected in the mobile phase is $\sigma_{a,0}^2 = l_a^2/12 + 2[\delta/(1 + k_m)]t$, where $l_a^2/12$ is the contribution due to the initial width of the solute. In order to quantify the

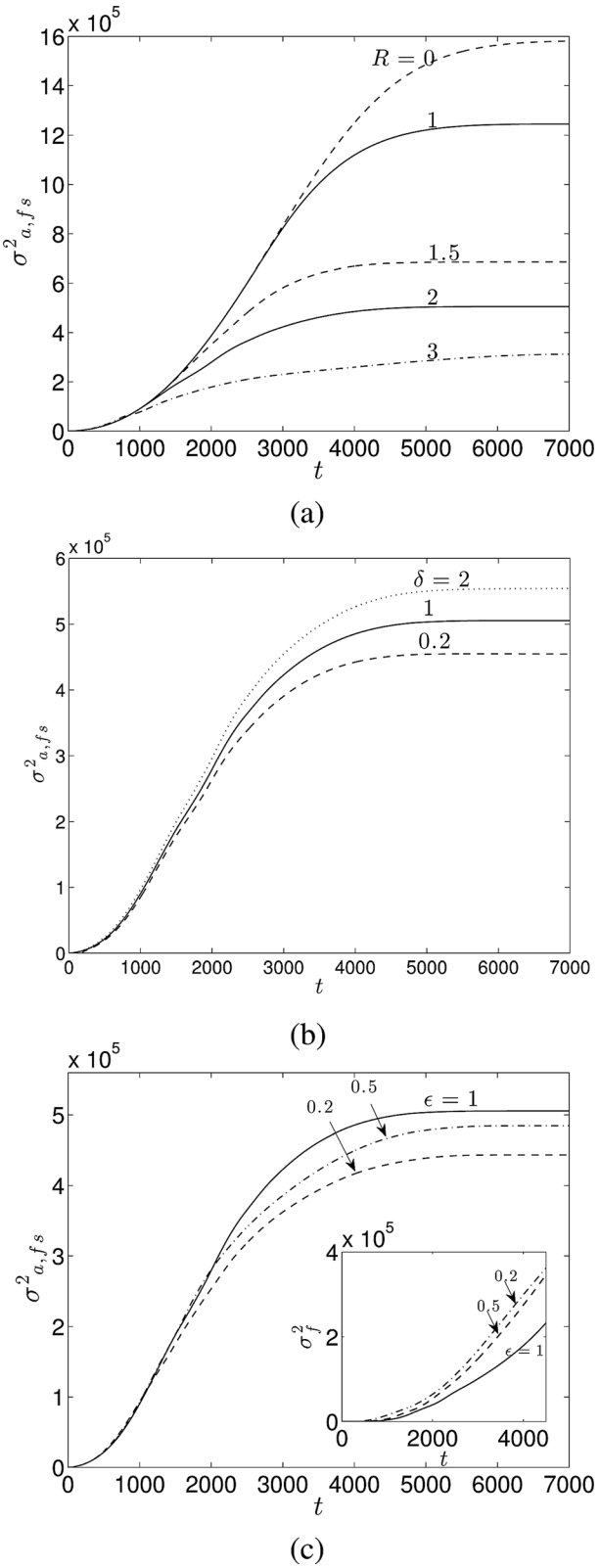


Fig. 8 Temporal evolution of the combined contributions of the solvent strength and VF effects to the solute variance, $\sigma_{a,fs}^2$, with $k_m = 5$, $S^* = 4$ (a) for different values of $R$ with $\delta = 1$, $\varepsilon = 1$, $\varepsilon_a = 1$. (b) for different values of $\delta$ with $R = 2$, $\varepsilon = 1$, $\varepsilon_a = 1$ (c) for different values of $\varepsilon$ with $k_m = 5$, $\delta = 1$, $\varepsilon_a = 1$, $S^* = 4$ and $R = 2$ (inset: temporal evolution of sample solvent variance for $R = 2$ and different values of $\varepsilon$).

contribution of the combined effects of VF and of the sample solvent strength on the total variance of the solute in the transient phase, $\sigma^2_{a,fs}$, can be computed as:

$$\sigma^2_{a,fs} = \sigma^2_a - \sigma^2_{a,0}. \quad (27)$$

In Fig. 8a the variance $\sigma^2_{a,fs}$ is plotted for different values of $R$ for $k_m = 5$ and $S^* = 4$. We see that $\sigma^2_{a,fs}$ increases gradually at early times and then saturates to a maximum value. This saturation time corresponds to the disengagement time of the solute zone from the sample solvent. The solute zone comes out of the influence of the fingering zone, hence the variance saturates to a maximum value under pure diffusive conditions. We see that the asymptotic variance of the solute decreases with an increase in the log mobility ratio $R$. This is because of the interplay and overall influence of the viscosity gradient and of the solvent strength effect on the solute dispersion. We know that, when increasing $R$, viscous fingering becomes intense and fingers travel faster.[14] Hence the variance of the sample solvent zone increases with an increase of the viscosity contrast between the sample solvent and the displacing fluid. However, the situation is quite different for the variance of the solute zone which is seen in Fig. 8a to decrease with increasing values of $R$. This can be explained by the fact that the advection speed of the locked-in part of the solute zone increases for larger values of $R$, whereas that of its dragged-along part is independent of $R$ along the upstream end. Therefore, the solute distribution width, and thus $\sigma^2_{a,fs}$, decreases with an increase in $R$.

Fig. 8b shows the influence of varying the ratio of the dispersion coefficients of the solute and of the sample solvent $\delta = D_a/D$ on $\sigma^2_{a,fs}$. For fixed value of $R$, $k_m$ and $S^*$, increasing $\delta$ has a destabilizing effect on the dynamics of the solute. For $\delta < 1$, $D > D_a$ so the sample solvent zone spreads faster. Hence the concentration of the sample solvent decreases faster with time which leads to an increase in $k(c)$. So the advection speed of the solute increases hence it comes out faster from the sample solvent. Thus $\sigma^2_{a,fs}$ is smaller for $\delta < 1$. However, for $\delta > 1$, $D_a > D$ the sample solvent is spreading at a slower rate thus its concentration decreases more slowly. So the advection speed of the solute is smaller, thus it is locked inside the sample solvent zone for a larger time. Hence it gets affected by the VF of the sample solvent for a longer time which results in an increase in its variance. Its saturation time also increases because of the increase in its disengagement time from the sample solvent zone with an increase in $\delta$. Hence we conclude that increasing $\delta$ induces a stronger influence of VF on the displacement of the solute.

The influence of the ratio of dispersion coefficients $\varepsilon$ on the variance profile of the solute is shown in Fig. 8c. We observe that the variance $\sigma^2_{a,fs}$ decreases when $\varepsilon$ decreases, which, for fixed values of $R$, has a destabilising effect on the sample solvent as VF is then more intense.[14] It is shown in the inset of Fig. 8c that the variance of the sample solvent zone increases with a decrease in $\varepsilon$. This is because a small transverse dispersion $D_y$ favours the longitudinal growth of VF of the sample solvent. But the situation is quite different with the analyte for which a decrease in $\varepsilon$ has a stabilising effect on the analyte dispersion dynamics. This is because the advection speed of the analyte zone locked in the sample solvent increases with a decrease in $\varepsilon$. So, the spreading of the solute distribution decreases with decreasing $\varepsilon$ which hence reduces the variance of the solute.

### 3.5 Propagation of longitudinal extrema of the solute fingers

Length average profiles of the local solute concentration, $\tilde{c}_a(y,t) = \frac{1}{L'}\int_0^{L'}(1+k(c))c_{a,m}(x,y,t)dx$ help in understanding the spreading of fingers and their interactions. In order to study the dynamics of the VF and solvent strength effects in the system, the space–time plots of the locations of the local extrema of these length average profiles are shown in Fig. 9b and d for $R =$ 1 and 3 (which correspond to simulations of Fig. 6b and d).

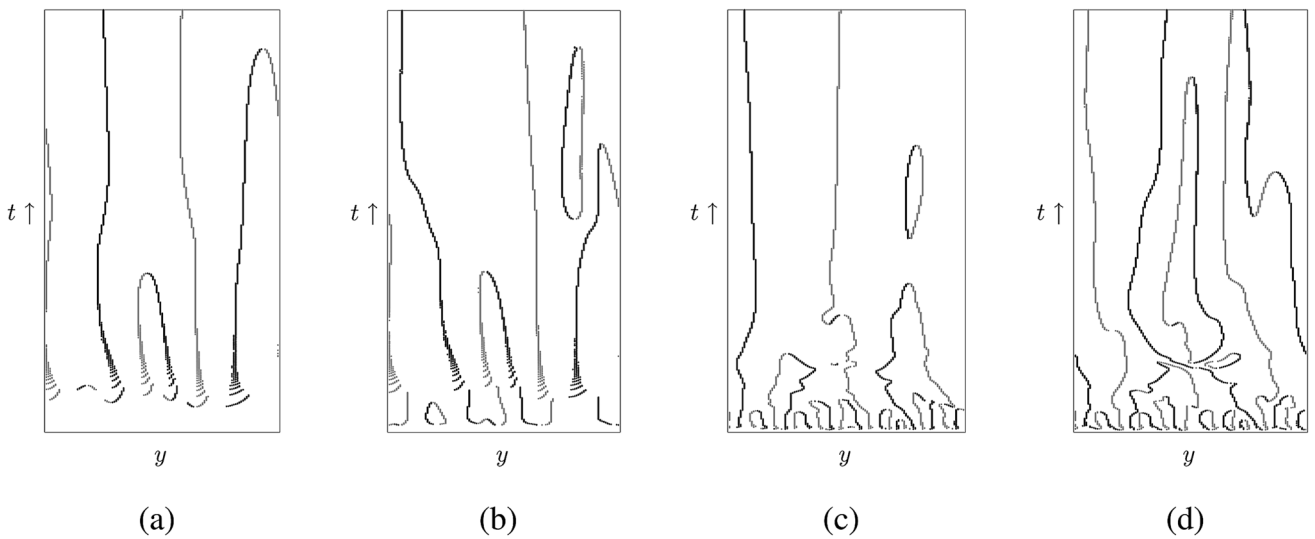


Fig. 9 Space-time plots of the longitudinal average profile of the sample solvent $\tilde{c}(y, t)$ and the solute $\tilde{c}_a(y, t)$ for parameters $k_m = 5$, $S^* = 4$, $\delta = 1$, $\varepsilon = 1$, $\varepsilon_a = 1$, (a) $\tilde{c}(y, t)$ for $R = 1$ (b) $\tilde{c}_a(y, t)$ for $R = 1$ (c) $\tilde{c}(y, t)$ for $R = 3$ (d) $\tilde{c}_a(y, t)$ for $R = 3$. Black represents maxima, grey represents minima.

Those for the sample solvent $\tilde{c}(y,t) = \frac{1}{L'}\int_0^{L'} c(x,y,t)\mathrm{d}x$ are shown in Fig. 9a and c respectively. Through space–time plots we show the mechanism of spreading and shielding of fingers along with the reordering of the extrema until one single finger remains. Here the horizontal direction corresponds to $y$ and time is increasing upwards from $t = 0$ to $t = 7000$. The defects in the space time plot are related to the death and birth of fingers.

The dynamics of the sample solvent (Fig. 9a) shows the presence of a large number of fingers at earlier times which start merging with time. In Fig. 9a we see that after a large time there is only one maximum–minimum which represents a single finger left when the dispersion dominates the system and dilutes the sample solvent into the bulk of displacing fluid. When the log mobility ratio $R = 1$, the viscosity difference between the sample solvent and the displacing fluid is relatively small. Thus, few fingers are seen in the dynamics of the sample solvent and hence in that of the solute (Fig. 6b). In the space–time plot there are few maxima and minima (see Fig. 9a and b) which ultimately merge to one single finger. Whereas with $R = 3$ (Fig. 9d), a large number of fingers is seen in the dynamics of the solute coinciding to the larger initial number of maxima and minima in the profiles of the sample solvent (Fig. 9c). The splitting of the solute fingers is dominant at earlier times and is later on taken over by a coarsening process due to a decrease in the effective viscosity ratio. For $R = 3$, splitting is more dominant than coarsening whereas the reverse is seen for $R = 1$. The dominance of coarsening at low values of $R$ (see Fig. 9) is evident from the spreading length $L_d$ of the solute which is larger for smaller $R$ due to merging of fingers as seen in Fig. 7b.

# 4 Conclusion

The spatio-temporal distribution of solutes entrained by a flow in a porous medium can become complex when affected by both VF and retention on the porous matrix. On one hand, VF due to a difference in viscosity between the sample solvent and the displacing fluid leads to a distortion of the solute profile which is widened and tailing. On the other hand, the fact that the degree of retention of the solutes on the porous matrix can depend on the local concentration of the sample solvent due to the solvent strength effect, can also lead to a bimodal distribution of the solutes in the column. When both effects are simultaneously at play, the retention varies strongly in space and time as it can be locally modulated by the fingering of the sample solvent.

In this article, we have presented the first description of solvent strengths effects on the distribution of adsorbed solutes with the presence of VF due to different viscosities of the sample solvent and of the displacing fluid in porous media. The model we have developed is a very general model which encompasses all previous effects studied separately. The problem is controlled by two main parameters, the log-mobility ratio $R$ due to the viscosities differences between sample solvent and displacing fluid and the solvent strength parameter $S^*$. We find that, in the absence of the solvent strength effect, *i.e.* setting $S^* = 0$, the adsorption of the solute reduces the effect of VF on it. On the other hand, adsorption with a solvent strength effect obtained when $S^* \neq 0$, increases the time of interaction of the solute with the VF of the sample solvent. We find that VF reduces the effect of the solvent strength on the solute distribution which decreases the bimodal character of the solute distribution. On the other hand, the spreading of the solute is reduced due to VF as compared to the case when only the solvent strength is playing a role. This anti-synergetic aspect of the interplay of the VF and solvent strength effects is counter-intuitive and has not been previously noticed to our knowledge. The main findings of the paper can thus be summarized as

- Both VF and a solvent modulated adsorption can affect the dynamics of solute propagation in porous media but when these effects are combined, they partially cancel each other.
- The bimodal distribution of the solute concentration, related to the solvent strength parameter $S^*$, vanishes as soon as the solute gets affected by VF of the sample solvent.
- The parametric study reveals that, when the log mobility ratio $R$ is increased, there is a decrease in the spreading length and an earlier disengagement of the solute zone.

The model presented here paves the way to a better understanding of peak deformations in chromatographic applications and possible quantitative comparison with experimental data in the presence of strong sample solvents. The equations we have presented may also be of future use in other applications including dispersion of solutes in soils and $CO_2$ sequestration where VF and variable retention are also encountered.

# Acknowledgements

M. Mishra gratefully acknowledges the financial support from the Department of Science and Technology, Government of India. A. D. acknowledges the support of the FRS-FNRS PDR project FORECAST.

# References

1 S. Hill, *Chem. Eng. Sci.*, 1952, **1**, 247–253.
2 P. G. Saffman and G. Taylor, *Proc. R. Soc. London, Ser. A*, 1958, **245**, 312–329.
3 G. M. Homsy, *Annu. Rev. Fluid Mech.*, 1987, **19**, 271–311.
4 Y. C. Yortsos, *J. Phys.: Condens. Matter*, 1990, **2**, SA443–SA448.
5 C. T. Tan and G. M. Homsy, *Phys. Fluids*, 1988, **31**, 1330–1338.
6 W. B. Zimmerman and G. M. Homsy, *Phys. Fluids A*, 1991, **3**, 1859–1872.
7 M. Czok, A. M. Katti and G. Guiochon, *J. Chromatogr.*, 1991, **550**, 705–719.
8 C. B. Castells and R. C. Castells, *J. Chromatogr. A*, 1998, **805**, 55–61.
9 T. T. Norton and E. J. Fernandez, *Ind. Eng. Chem. Res.*, 1996, **35**, 2460–2468.
10 H. J. Catchpoole, R. A. Shalliker, G. R. Dennis and G. Guiochon, *J. Chromatogr. A*, 2006, **1117**, 137–145.

 

11 G. Guiochon, A. Felinger, D. G. Shirazi and A. M. Katti, *Fundamentals of Preparative and Nonlinear Chromatography*, Academic Press, 2006.
12 R. A. Shalliker and G. Guiochon, *Analyst*, 2010, **135**, 222–229.
13 C.-Y. Chen and S.-W. Wang, *Int. J. Numer. Methods Heat Fluid Flow*, 2001, **11**, 761–778.
14 A. De Wit, Y. Bertho and M. Martin, *Phys. Fluids*, 2005, **17**, 054114.
15 S. Keunchkarian, M. Reta, L. Romero and C. Castells, *J. Chromatogr. A*, 2006, **1119**, 20–28.
16 G. Rousseaux, M. Martin and A. De Wit, *J. Chromatogr. A*, 2011, **1218**, 8353–8361.
17 M. Mishra, M. Martin and A. De Wit, *Phys. Rev. E: Stat., Nonlinear, Soft Matter Phys.*, 2008, **78**, 066306.
18 M. L. Dickson, T. T. Norton and E. J. Fernandez, *AIChE J.*, 1997, **43**, 409–418.
19 M. Mishra, M. Martin and A. De Wit, *Phys. Fluids*, 2009, **21**, 083101.
20 M. Mishra, M. Martin and A. De Wit, *Chem. Eng. Sci.*, 2010, **65**, 2392–2398.
21 P. Jandera and G. Guiochon, *J. Chromatogr.*, 1991, **588**, 1–14.
22 T.-L. Ng and S. Ng, *J. Chromatogr.*, 1985, **329**, 13–24.
23 M. Mishra, C. Rana, A. De Wit and M. Martin, *J. Chromatogr. A*, 2013, **1297**, 46–55.
24 L. R. Snyder, J. W. Dolan and J. R. Gant, *J. Chromatogr.*, 1979, **165**, 3–30.
25 J. Bear, *Dynamics of Fluids in Porous Media*, Dover Publications, 1988.
26 C. Canuto, M. Y. Hussaini, A. Quarteroni and T. A. Zang, *Spectral Methods in Fluid Dynamics*, Springer-Verlag, 1988.
27 L. N. Trefethen, *Finite Difference and Spectral Methods for Ordinary and Partial Differential Equations*, 1996, unpublished text, available at http://people.maths.ox.ac.uk/trefethen/pdetext.html.
28 N. E. Hoffman, S.-L. Pan and A. M. Rustum, *J. Chromatogr.*, 1989, **465**, 189–200.